Mapping Concentration Profiles within the Diffusion Layer of an Electrode: Application to Redox Catalysis

Christian Amatore,*[a] Cécile Pebay,[a] Onofrio Scialdone,[b] Sabine Szunerits,[a] and Laurent Thouin[a]

Abstract: Catalytic reductions of some aromatic halides were performed at a millimetric electrode with several redox mediators. The resulting concentration profiles were monitored amperometrically by placing an ultramicroelectrode inside the diffusion layer produced at the former electrode. The features of redox catalysis and the subsequent structuring of the diffusion layer were investigated experimentally under steady-state conditions imposed by the spontaneous convection of the solution. The concentration profiles established from the probe measurements were in agreement with our theoretical predictions, based on fast kinetics of redox catalysis. Under these conditions, very similar to preparative electrosynthesis, the diffusion layer separates into two domains where pure diffusion takes place and the concentration profiles therein are mainly linear. We demonstrate that the limit between these two zones does not depend on kinetics, but is rather fixed by the product of the ratio of the bulk concentrations of each species and the ratio of their diffusion coefficients.

Keywords: catalysis · concentration profile · diffusion layer · electrochemistry · microelectrode

Introduction

Redox catalysis provides the means of electrochemically activating a substrate, S, at a potential located far before (i.e., positive to in reduction, or negative to in oxidation) its electrochemical wave.[1–3] This is performed through the use of an electron-transfer mediator, M, whose chemically stable reduced or oxidized form $M^{\bullet\pm}$ accordingly [Eq. (1)] is able to transfer an electron endergonically to the substrate, S [Eq. (2)]. When the resulting activated substrate $S^{\bullet\pm}$ is sufficiently chemically unstable [Eq. (3)], the up-hill equilibrium in Equation (2) is pulled continuously to the right so that $S^{\bullet\pm}$ is continuously generated at a maximum rate imposed by the forward rate constant of Equation (2):

$$M \pm e^- \rightarrow M^{\bullet\pm} \quad (1)$$

$$M^{\bullet\pm} + S \rightarrow M + S^{\bullet\pm} \quad (k) \quad (2)$$

$$S^{\bullet\pm} \rightarrow etc. \quad (3)$$

[a] Dr. C. Amatore, C. Pebay, Dr. S. Szunerits, Dr. Laurent Thouin
Ecole Normale Supérieure
Département de Chimie, UMR CNRS 8640 "*PASTEUR*"
24 rue Lhomond, 75231 Paris cedex 05 (France)
Fax: (+33) 1-44-32-33-25
E-mail: amatore@ens.fr

[b] Dr. O. Scialdone
Engenieria di Palermo, Viale delle Scienze
90128 Palermo (Italy)

The fundamental kinetic reasons explaining why the rate of the follow-up reaction [Eq. (3)] may be sufficient to pull the homogeneous electron transfer at a significant rate have been well discussed previously, since the same reaction does not succeed in doing so when the substrate is reduced or oxidized directly at the potential of the redox mediator.

Redox catalysis has been shown to be extremely useful for determining the standard potential of a variety of $S/S^{\bullet\pm}$ redox couples, or the rate constant of $S^{\bullet\pm}$ fast chemical evolution [Eq. (3)], for substrates for which direct measurements would have been impossible even with the fastest available direct electrochemical techniques. In such investigations, one adjusts the time scale of the electrochemical experiment so that it becomes comparable to the rate of regeneration of M [Eqs. (2) and (3)]. In other words, in these kinetic experiments, the electrochemical time scale is made sufficiently short for the process in Equations (2) and (3) to be incomplete. The turn-over of the whole process then decays upon decreasing the time-scale and its variations can be measured precisely, so that the forward rate constant representing the sequence of Equations (2) and (3) may be determined.

In contrast, when one uses redox catalysis for preparative purposes, a large turn-over is desired in order that a small fraction of redox mediator afford a current density comparable to that which would be obtained for direct electrolysis of the substrate. As a consequence, the overall kinetics of the

  0947-6539/01/0713-2933 $ 17.50+.50/0

process in Equations (2) and (3) need to be much larger than the rate of diffusion of $M^{\bullet\pm}$ from the electrode surface to the solution bulk. Under such conditions $M^{\bullet\pm}$ cannot survive enough to escape from the diffusion layer towards the solution bulk. Similarly, S cannot survive its penetration into the diffusion layer up to the electrode surface. $M^{\bullet\pm}$ and S then cannot coexist in the diffusion layer, except within a narrow strip of solution that separates two distinct zones of the diffusion layer (Figure 1a). One zone, adjacent to the electrode surface contains M and $M^{\bullet\pm}$ and no S or $S^{\bullet\pm}$. The other zone, located between this narrow strip and the solution bulk contains only M and S. $M^{\bullet\pm}$ and S may then react together [Eqs. (2) and (3)] only within the excessively narrow domain which separates the above two zones. In this narrow strip of solution $M^{\bullet\pm}$ and S have then necessarily extremely small concentrations.

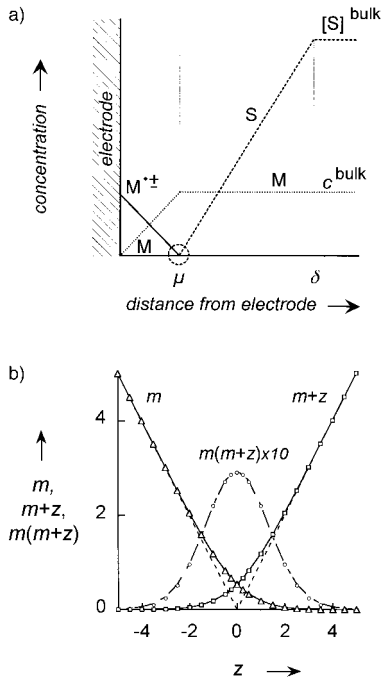

Figure 1. a) Theoretical concentration profiles during the catalytic oxidation (or reduction) of the substrate S by the radical cation (or radical anion) of the mediator $M^{\bullet\pm}$; b) Zoom of the concentrations resolved numerically around $y=\mu$ (zone marked by the circle in a), m and $m+z$ are the dimensionless concentrations of the mediator radical $M^{\bullet\pm}$ and substrate S respectively, $m(m+z)$ corresponds to the dimensionless form of the kinetic term in Equation (9) (Note that the profile shown is a 10-times-expanded vertical scale). $z=\lambda^{1/3}[(y/\mu)-1]$ where y is the distance from the electrode (see text for the meaning of the dimensionless rate constant λ), $m=[M^{\bullet\pm}]/c^{bulk}$, and $m+z=|n|(D_S/D_M)[S]/c^{bulk}$.

This spontaneous kinetic structuring of a diffusion layer has been pointed out since the earliest kinetic investigations of redox catalysis, but much less emphasis has been put on this phenomenon than on the highly interesting kinetic applications of the method. Since, by definition, rather short time scales need to be used in these kinetic applications (vide supra), $M^{\bullet\pm}$ survives within almost the whole much shorter diffusion layers thus created. Similarly, S penetrates the diffusion layer upto the electrode surface, since the chemical toll due to Equation (2) is small compared with the short time scale. Therefore, $M^{\bullet\pm}$ and S coexist over a significant fraction of these extremely short diffusion layers, so that the above structuring does not occur. This may lead to the intuitive view that in redox catalysis $M^{\bullet\pm}$ and S always react together in an almost homogeneous fashion, both species being then distributed within the whole diffusion layer, although this cannot occur under realistic preparative conditions as recalled above and will be established thoroughly in the theoretical section of this paper.

We wish to show hereafter that, thanks to the development of in situ mapping techniques developed recently in our laboratory,[4–7] the precise concentration profiles of $M^{\bullet\pm}$ and S can be monitored so as to establish definitively the existence of the above diffusion-layer structuring when redox catalysis is performed under conditions that are similar to those occurring within a realistic preparative electrolysis. Because of this latter concern, all the experiments reported here are performed under steady-state conditions as imposed by spontaneous convection (Nernst layer conditions).

Results and Discussion

Theory: To further clarify the above notion of the diffusion-layer structuring, we wish first to elaborate upon the conditions under which this essential feature of redox catalysis takes place. For this we consider that $M^{\bullet\pm}$ is produced at the electrode upon electrolysis of M on its current plateau [Eq. (1)]. Upon diffusing towards the extremity of the diffusion layer, $M^{\bullet\pm}$ meets an opposite flux of S, which is diffusing in the direction of the electrode. We assume hereafter that both species react together sufficiently fast [Eq. (2)], that either species annihilates the other one in any solution domain where its concentration dominates (Figure 1a). This occurs when $kc^{bulk}\delta^2/D_S \gg 1$, where c^{bulk} is the catalyst bulk concentration, δ is the steady state diffusion layer thickness and D_S the diffusion coefficient of S. Then the two species may exist simultaneously only within a thin strip of solution located somewhere in the midst of the diffusion layer. Let μ be the distance of this thin domain from the electrode surface, and 2Δ its thickness. As will be shown below, μ is independent of $kc^{bulk}\delta^2/D_S$, while Δ is very small compared with μ or δ, provided that $kc^{bulk}\delta^2/D_S \gg 1$ (vide infra). Thus, when the reaction in Equation (2) is fast enough, S cannot enter the domain near the electrode surface where $M^{\bullet\pm}$ dominates (namely, $[S]=0$ for $y<\mu-\Delta$, y being the distance to the electrode surface). Conversely, $M^{\bullet\pm}$ cannot enter the other domain of the diffusion layer where S dominates (namely, $[M^{\bullet\pm}]=0$ for $\mu+\Delta<y<\delta$). In either region neither species can react due to the absence of the other, so that it undergoes pure diffusion and its concentration profile in the region is linear under steady-state conditions.

We consider hereafter that $S^{\bullet\pm}$, which is produced exclusively within the narrow domain separating the diffusion layers, evolves extremely fast to a final species, P, possibly after a cascade of $|n|-1$ electron transfers and chemical steps following the reaction of Equation (2):

$$S^{\bullet\pm}[+\ (|n|-1)M^{\bullet\pm}+\ \ldots] \rightarrow P\ [+\ (|n|-1)M+\ \ldots] \qquad (4)$$

0947-6539/01/0713-2934 $ 17.50+.50/0 *Chem. Eur. J.* **2001**, *7*, No. 13

so that the electron transfer in Equation (2) is the rate determining step of the overall balance equation shown in Equation (5):

$$|n|(\mathrm{M}\pm\mathrm{e}^-)+\mathrm{S}+etc\rightarrow|n|\ \mathrm{M}+\mathrm{P}+etc \tag{5}$$

When the electrode potential is poised on the plateau of the redox catalyst wave, the flux of $M^{\cdot\pm}$ at $y=\mu-\Delta$ is $-D_M c^{bulk}/(\mu-\Delta)\approx -D_M c^{bulk}/\mu$ in which D_M the diffusion coefficient of M. At the same instant, the flux of S at $y=\mu+\Delta$ is $D_S[S]^{bulk}/(\delta-\mu-\Delta)\approx D_S[S]^{bulk}/(\delta-\mu)$. The stoichiometry in Equation (5) imposes that at μ the modulus of flux of $M^{\cdot\pm}$ is $|n|$ times that of S. This condition immediately defines the value of μ:

$$\mu=\frac{\delta}{1+\dfrac{|n|D_S[S]^{bulk}}{D_M c^{bulk}}} \tag{6}$$

Equation (6) shows that μ does not depend on kinetics, but is fixed only by the ratio of the bulk concentrations of each species times their diffusion coefficients. This equation also affords the current, which flows through the electrolytic cell. Indeed, since $M^{\cdot\pm}$ diffuses without reacting in the domain $0<y<\mu$, under steady-state conditions its concentration profile is linear, so that $(\partial[M^{\cdot\pm}]/\partial y)_{y=0}\approx c^{bulk}/\mu$ provided that the electrode potential is poised on the plateau of the $M/M^{\cdot\pm}$ wave. From Fick's first law, the absolute value of the current is $I=\pm FAD_M(\partial[M^{\cdot\pm}]/\partial y)_{y=0}$, in which A is the electrode surface area [Eq. (7)].

$$I=\frac{\pm FAD_M c^{bulk}}{\mu}=\pm\frac{FAD_M c^{bulk}}{\delta}\times\left(1+\frac{|n|D_S[S]^{bulk}}{D_M c^{bulk}}\right) \tag{7}$$

Note that in the absence of substrate, S, the current would be $I_0=\pm(FAD_M c^{bulk}/\delta)$, which corresponds to the reaction in [Eq. (1)]. It ensues that the catalytic Faradaic efficiency is:

$$\varepsilon_F=\frac{I}{I_0}=\frac{\delta}{\mu}=1+\frac{|n|D_S[S]^{bulk}}{D_M c^{bulk}} \tag{8}$$

Interestingly, this shows that ε_F does not depend on the rate of the electron-transfer reaction in Equation (2) as soon as this is fast enough; that is, provided that Δ is small enough compared with δ.

Let us now clarify this point by working out the value of Δ. For this, we need to establish the concentration profiles of $M^{\cdot\pm}$ and S within the thin domain of thickness 2Δ located around μ, where both species coexist. Owing to the balance in Equation (5), one has at any point within the diffusion layer (namely, $0<y<\delta$):

$$D_M\frac{\partial[M^{\cdot\pm}]}{\partial y^2}=|n|D_S\frac{\partial^2[S]}{\partial y^2}=|n|k[M^{\cdot\pm}][S] \tag{9}$$

It then follows that:

$$D_M[M^{\cdot\pm}]-|n|D_S[S]=D_M c^{bulk}(1-y/\mu) \tag{10}$$

This shows that $[M^{\cdot\pm}]/c^{bulk}$ is the solution of the dimensionless equation:

$$\frac{\partial^2[M^{\cdot\pm}]/c^{bulk}}{\partial(y/\mu)^2}=\lambda\frac{[M^{\cdot\pm}]}{c^{bulk}}\left(\frac{[M^{\cdot\pm}]}{c^{bulk}}+\left(\frac{y}{\mu}-1\right)\right) \tag{11}$$

in which $\lambda=(kc^{bulk}\mu^2/D_S)$ is a dimensionless rate constant. Let us then introduce the two following dimensionless variables:

$$space: \qquad z=\lambda^{1/3}\left(\frac{y}{\mu}-1\right)=\left(\frac{y}{\mu}-1\right)\left(\frac{kc^{bulk}\mu^2}{D_S}\right)^{1/3} \tag{12}$$

$$concentration: \quad m=\lambda^{1/3}\left(\frac{[M^{\cdot\pm}]}{c^{bulk}}\right)=\left(\frac{[M^{\cdot\pm}]}{c^{bulk}}\right)\left(\frac{kc^{bulk}\mu^2}{D_S}\right)^{1/3} \tag{13}$$

so that Equation (11) becomes:

$$\partial^2 m/\partial z^2=m(m+z) \tag{14}$$

When $\lambda\rightarrow\infty$, this dimensionless second-order differential equation is associated with the following boundary conditions:

$$z\rightarrow-\infty: \qquad m\rightarrow -z \tag{15}$$

$$z\rightarrow+\infty: \qquad m\rightarrow 0 \tag{16}$$

Equation (14) and its two boundary conditions are independent of any parameter. This is an extremely important feature, since it shows that the solution $m(z)$ of this system is unique whatever the values of the parameters which define the experimental kinetic problem at hand are. In particular, the symmetry of the system establishes that $\kappa=m(m+z)$, which is the dimensionless form of the kinetic term in Equation (9), passes through a finite maximum κ_{max} at $z=0$, and tends towards zero for $|z|\gg\sigma_\Delta$, where σ_Δ is a finite constant to be determined below. This is tantamount to saying mathematically what we summarized in Figure 1a. Indeed, because of the definitions of z and m in Equations (12) and (13), this amounts to expressing that when $kc^{bulk}\delta^2/D_S\gg 1$ (namely, $\lambda\gg 1$), $M^{\cdot\pm}$ and S diffuse freely in all the diffusion layer domains where they exist, except within a narrow strip located around $y=\mu$ (i.e., around $z=0$) of an extremely small thickness 2Δ (namely, $\Delta\sim\sigma_\Delta\lambda^{-1/3}\rightarrow 0$).

Therefore, M may be regenerated and $S^{\cdot\pm}$ produced only within this thin kinetic strip. In other words, contrary to the generally spread, intuitive picture of redox catalysis that occurs by the overlap of M and $S^{\cdot\pm}$ concentration profiles over a significant fraction of the diffusion layer, the true redox catalytic phenomenon occurs only within an extremely narrow domain located around $y=\mu$, in the midst of the diffusion layer. The two other remaining portions of the diffusion layer then only play the role of kinetically inert diffusional "feeders", whose role is only that of delivering the two reactants, $M^{\cdot\pm}$ and S, to the very small region where they react together. These conclusions cannot be drawn when $kc^{bulk}\delta^2/D_S$ (namely, λ) is not large enough for Δ to be smaller than δ. However, this defines conditions under which the redox catalytic procedure is almost inactive and is therefore not suitable from a preparative point of view. It follows that any system that presents a preparative interest necessarily behaves as sketched in Figure 1a.

To proceed quantitatively, the system of the differential Equation (14) and its boundary conditions [Eqs. (15) and (16)] need to be solved. This was performed numerically through a classical finite-differences procedure. The results are shown in Figure 1b, which zooms over the region around

$y = \mu$ marked by the circle in Figure 1a. Figure 1b confirms that σ_Δ is finite and that its maximum value is of a few units only. For example by defining σ_Δ so that more than 99% of the $S^{\bullet\pm}$ production and M regeneration [Eq. (2)] occurs within the domain $|z| \leq \sigma_\Delta$, $\sigma_\Delta \approx 3.7$ is obtained. σ_Δ becomes only about 2.2 when the domain is defined so that 90% of $S^{\bullet\pm}$ is produced and M regenerated within its boundaries.

Since σ_Δ is found to be close to unity, it results from Equation (12) that in the real space, y, the thickness $2\Delta = 2\sigma_\Delta \mu \lambda^{-1/3}$ of the narrow domain in which $M^{\bullet\pm}$ and S coexist tends towards zero as $\lambda^{-1/3}$ does. Equation (6) shows that this extremely small domain is located within the diffusion layer at a distance μ/δ, which depends only on the relative diffusion coefficients and bulk concentrations of the substrate and redox mediator. Outside of this interfacial domain, $M^{\bullet\pm}$ and S diffuse in their zone of predominance so that their concentration profiles are linear therein (Figure 1).

To conclude this section, let us examine more precisely when this situation arises. In practice, the system will behaves as sketched in Figure 1 provided that Δ is a small fraction, ρ, of μ. Since $\Delta = \sigma_\Delta \mu \lambda^{-1/3}$, this imposes that $\rho = \sigma_\Delta \lambda^{-1/3} \ll 1$, that is, that $kc^{bulk}\mu^2/D_S \gg \sigma_\Delta{}^3$. For most preparative situations of interest, μ^2/D_S is of the order of a few tens of seconds, so that from the above σ_Δ values, it follows that these results apply whenever kc^{bulk} is larger than a few reciprocal seconds. Considering that in any realistic situation c^{bulk}, the concentration of the catalyst, is at least in the millimolar range; this means that the above results always apply whenever k, the forward rate constant of the electron transfer in Equation (2), is larger than $10^3\,M^{-1}\,s^{-1}$. On the other hand, by the definition of redox catalysis, this reaction has a positive ΔG^0 equal to $F\Delta E^0$, in which ΔE^0 is the absolute difference between the standard redox potentials of the substrate and of the redox mediator, so that $k \approx k_{dif}\exp(-F\Delta E^0/RT)$, where k_{dif} is the diffusion limit rate constant. Under usual conditions this later is in the range of $10^9 \sim 10^{10}\,M^{-1}\,s^{-1}$, so that the above condition on k is equal to saying that our results always apply, provided that ΔE^0 does not exceed 0.35 to 0.40 V. Again this corresponds to usual situations in preparative scale electrolysis. Therefore, our above results and conclusions appear to correctly describe almost any realistic preparative situations involving a redox catalytic procedure.

Experimental illustrations: We took as an illustration the catalytic reduction of an aromatic halide (ArX), which involves the anion radical of the starting molecule as intermediate. The reductive cleavage of the carbon–halogen bond is one of the simplest examples of such a process in organic electrochemistry. Even though the anion radical formed upon injection of one electron appears as a true intermediate in most cases [Eq. (18)], it may cleave very rapidly into the corresponding aryl radical and the halide ion [Eq. (19)]. According to the definition given above, the redox catalysis takes place when the electrochemical generation of the reduced form $M^{\bullet-}$ of a reversible and chemically stable redox couple $M/M^{\bullet-}$, is performed at a potential positive to the reduction of ArX [Eq. (17)]:

$$M + e^- \leftrightarrow M^{\bullet-} \quad (17)$$

$$M^{\bullet-} + ArX \leftrightarrow M + ArX^{\bullet-} \quad (18)$$

$$ArX^{\bullet-} \leftrightarrow Ar^{\bullet} + X^- \quad (19)$$

The neutral radical $Ar^{\bullet}$ thus formed may then be reduced at the electrode [Eq. (20)] or in solution [Eq. (21)]; this leads, after protonation by the solvent, the residual water or the quaternary ammonium cation of the supporting electrolyte, to ArH [Eq. (22)].

$$Ar^{\bullet} + e^- \leftrightarrow Ar^- \quad (20)$$

$$Ar^{\bullet} + ArX^{\bullet-} \rightarrow ArX + Ar^- \quad \text{and/or} \quad Ar^{\bullet} + M^{\bullet-} \rightarrow Ar^- + M \quad (21)$$

$$Ar^- + H^+ \rightarrow ArH \quad (22)$$

Under such conditions, the main process will then appear as a two-electron reduction process provided that the lifetime of the anion radical is sufficiently short. The reduction of the next three aromatic halides, iodobenzene ($E^0 = -2{,}1$ V vs. SCE), 2-bromonaphthalene ($E^0 = -2.2$ V vs. SCE), and 2-bromopyridine ($E^0 = -2.34$ V vs. SCE) follow this chemical pathway.[8, 9] To establish experimentally the concentration profiles that take place at the electrode surface during the catalytic reduction, several redox mediators were investigated whose standard potentials were in the range of potentials mentioned above, that is, E^0 not higher than 0.5 V from the standard potentials of the aromatic halides: benzophenone ($E^0 = -1.75$ V vs. SCE), 1-cyanonaphthalene ($E^0 = -1.78$ V vs. SCE), 1,3-diphenylisobenzofuran ($E^0 = -1.82$ V vs. SCE), methyl benzoate ($E^0 = -2.17$ V vs. SCE) and perylene ($E^0 = -1.63$ V vs. SCE).

A disc electrode (generator) of millimetric dimension was used to locally generate the concentration gradients. Before any measurements were made, this electrode was polarized for several seconds until the steady state regime imposed by the natural convection of the solution was reached. The resulting concentration profiles were then monitored by placing a platinum-disk ultramicroelectrode (probe) at selected positions within the diffusion layer of the generator electrode. An amperometric detection was performed according to the details reported in the Experimental Section that allowed a direct evaluation of the concentrations of the target species.[7]

Figure 2 shows two concentration profiles recorded by the probe when iodobenzene (ArX) is added to a solution initially containing 5 mM of benzophenone (M). The generator was poised at a potential $E_1 = -1.95$ V vs. SCE, between the half-wave potential of benzophenone and iodobenzene. For each measurement, the probe was connected after a time delay of 50 s so that the generator reached its steady state current. The probe potential was set either at potential $E_0 = 0$ V vs. SCE, namely, on the oxidation wave of the benzophenone radical anion or at potential E_1. In the latter case, it corresponds either to the reduction of benzophenone for solutions only containing benzophenone or to the catalytic reduction of iodobenzene for solutions of benzophenone and iodobenzene. For each distance all currents monitored at the probe after a sampling time, θ, were normalized to the value i_0, measured with the same probe by applying a potentiostatic step of

0947-6539/01/0713-2936 $ 17.50+.50/0 *Chem. Eur. J.* **2001**, *7*, No. 13

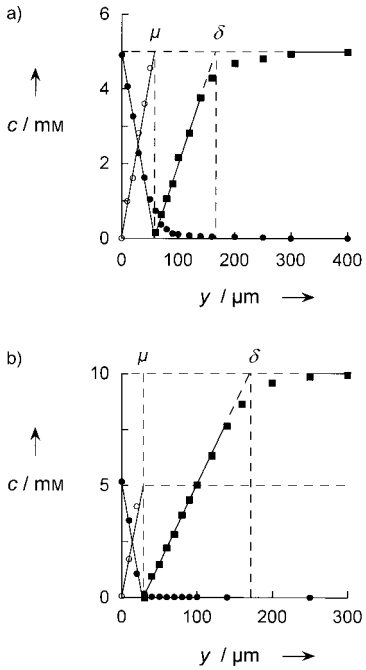

Figure 2. Catalytic reduction of iodobenzene by benzophenone. Concentration profiles monitored by the probe electrode in 0.1M nBu_4NBF_4/DMF: a) 5mM benzophenone + 5mM iodobenzene; b) 5mM benzophenone + 10 mM iodobenzene: benzophenone (○), benzophenone radical anion (●), iodobenzene (■).

identical duration at potential E_1 in a bulk solution only containing benzophenone.

The concentrations of both forms of the mediator (i.e., M and $M^{\bullet -}$) were then readily obtained by the following equations:

$$0 < y < \mu \qquad c_M(y) = \left[\frac{i(\theta, E_1, y)}{i_0}\right] \times c^{bulk} \tag{23}$$

$$0 < y \qquad c_{M^-}(y) = \left[\frac{i(\theta, E_0, y)}{i_0}\right] \times \left(\frac{D_M}{D_{M^-}}\right)^{1/2} c^{bulk} \tag{24}$$

here c_{M^-} and D_{M^-} are, respectively, the concentration and diffusion coefficients of $M^{\bullet -}$. According to the structure of the diffusion layer expected in such a case (Figure 1a) Equation (24) applies over all distances, since the probe current monitored at potential E_0 is indicative only of the concentration of $M^{\bullet -}$, whatever the local composition. On the other hand, Equation (23) is only valid over a restricted range of distances (i.e., $y < \mu$) corresponding to the location in the diffusion layer where the concentration gradient of the mediator is produced. Indeed, at higher distances (i.e., $y > \mu$) the aromatic halide is simultaneously detected by the probe; this prevents any straightforward determination of the concentration of the mediator itself.

However, even if redox catalysis takes place at the probe under such conditions (i.e., probe polarized at E_1 and distances $y > \mu$) it affords a way to monitor the concentration gradient of the aromatic halide alone. Indeed, as long as the catalytic process is fast enough and controlled by diffusion, the probe current is a sum of two contributions [Eq. (7)] due on one side to the reduction of the mediator and on the other side to the two-electron reduction of the aromatic halide. For catalytic currents recorded after a short sampling time, θ, Equation (7) can be rewritten as Equation (25). The concentration of the aromatic halide is then readily obtained by Equation (26) provided that the concentration of the mediator is assumed to be constant over distances, y, higher than μ and equal to c^{bulk} (Figure 1a):

$$y > \mu \qquad i(\theta, E_1, y) = \frac{FA}{(\pi\theta)^{1/2}}[D_M{}^{1/2} c^{bulk} + 2 D_{ArX}{}^{1/2} C_{ArX}(y)] \tag{25}$$

$$y > \mu \qquad C_{ArX}(y) = \left[\frac{i(\theta, E_1, y) - i_0}{2 i_0}\right] \times \left(\frac{D_M}{D_{ArX}}\right)^{1/2} c^{bulk} \tag{26}$$

Based on the probe current measurements and Equations (23), (24) and (26), all the three concentration profiles (namely, of M, $M^{\bullet -}$ and ArX) can be determined by using the diffusion coefficient values which were preliminarily estimated (see Experimental Section below). Figure 2 shows qualitatively the influence of the iodobenzene concentration, for a fixed concentration of benzophenone in solution. One can observe that these profiles are in good agreement with our predictions (Figure 1a). Each set of data is self-consistent within the precision of the measurements, since both concentrations of benzophenone and iodobenzene tend to zero at approximately the same location μ within the diffusion layer. Furthermore, an increase in the concentration of iodobenzene results experimentally in a decrease of the distance, μ, which agrees qualitatively with Equation (6).

The effect of the concentration of the aromatic halide on the position of μ is better seen in Figure 3a, which shows the concentration profiles of the radical anion of benzophenone

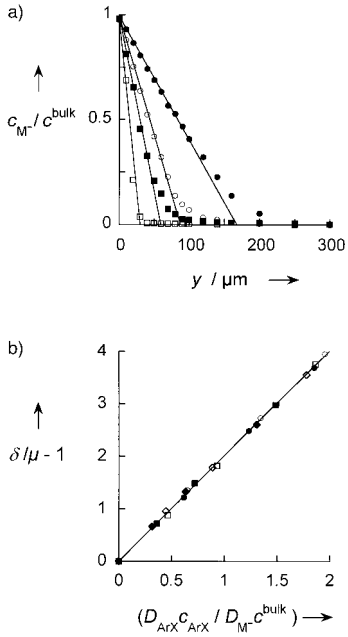

Figure 3. a) Concentration profiles of the benzophenone radical anion during the catalytic reduction of iodobenzene. Influence of the addition of iodobenzene to a solution of 10mM benzophenone in 0.1M nBu_4NBF_4/DMF: [PhI] = 0mM (●), 2.5mM (○), 5mM (■), 10mM (□); b) Correlation between $\delta/\mu - 1$ and c_{ArX}/c^{bulk} (slope = 2.004, $R^2 = 0.9995$): iodobenzene + perylene (○), iodobenzene + benzophenone (●), 2-bromonaphthalene + 1,3-diphenylisobenzofuran (□), 2-bromonaphthalene + 1-cyanonaphthalene (■), 2-bromopyridine + 1-cyanonaphthalene (◇), 2-bromopyridine + methyl benzoate (◆).

for concentrations of iodobenzene ranging from 0 to 10 mM. Without addition of iodobenzene, the concentration profile is linear over 75% of the concentration gradient, according to the classical Nernst layer approximation. At higher distances, a deviation from linearity is observed reflecting the progressive involvement of spontaneous convection of the solution as already discussed in detail.[10] The thickness, δ, of the diffusion layer can be calculated by extrapolating the linear dependence of the concentrations observed near the electrode surface to a zero intercept. In those experimental conditions, δ is estimated at 175 μm (Figure 3a). One must stress that the same thickness is roughly obtained from Figure 2a and b by extrapolating the concentrations of iodobenzene at larger distances. All these values also compare very well to those we determined previously for pure diffusion in motionless solutions.[6, 7] Provided that the experimental set up is rather similar, spontaneous convection is fixed exclusively by external vibrations, movement of air near the cell, etc. In particular, we demonstrated[10] that close to the electrode surface, the convective contribution decreases extremely fast and transport of molecules to/from the electrode occurs only by true diffusion. The concentration gradient of the mediator, which takes place closer to the electrode as more iodobenzene is added (Figure 3a), is accordingly less altered by spontaneous convection. Experimentally it leads to a linear variation of the concentration of the benzophenone radical anion of up to 90% of its whole gradient.

By plotting $[(\mu/\delta - 1)]$ versus the concentration ratio of substrate over mediator, a linear correlation is expected from Equation (6) depending on the respective diffusion coefficients:

$$\left(\frac{\mu}{\delta} - 1\right) = 2 \times (D_{ArX}/D_{M^-}) \times (c_{ArX}/c^{bulk}) \quad (27)$$

Equation (27) was verified experimentally for several combinations between the three aromatic halides and the five mediators mentioned above (Figure 3b). In each case, the concentration profiles were established for different concentrations of substrate and mediator according to the diffusion coefficients previously determined (see Experimental Section). A very good correlation was obtained within the precision of the measurements, the experimental slope being equal to two as predicted by Equation (27).

Conclusion

In this work, thanks to the possibility of monitoring concentration profiles in situ on the micrometric scale, we have demonstrated the features of redox catalysis under conditions which are appropriate for preparative purposes. As the overall chemical kinetics of the process are fast compared with diffusion under these conditions, the concentration profiles of the mediator and substrate are fixed exclusively by the diffusion rate of the two reacting species; this leads to a specific kinetic structuring of the diffusion layer. In agreement with the theoretical predictions, the diffusion layer separates into two domains, the limit between each zone being set by the condition of identical fluxes for each reacting species. This particular structuring of the diffusion layer is, however, not specific to redox catalysis but could be met for different kind of processes. Indeed, this diffusion pattern is also expected for reactions between solvated electrons produced by a reducing metal and substrates[11] and also occurs at second waves of EE mechanisms.[4]

Experimental Section

Chemicals: All solutions were prepared in DMF (Carlo Erba) with 0.1M tetrabutylammonium tetrafluoroborate as the supporting electrolyte. The catalytic reduction of the three following aromatic halides was investigated: iodobenzene (Fluka), 2-bromonaphathalene (Aldrich) and 2-bromopyridine (Aldrich). Five mediators were used: benzophenone (Aldrich), 1-cyanonaphthalene (Aldrich), 1,3-diphenylisobenzofuran (Aldrich), methyl benzoate (Aldrich) and perylene (Aldrich).

Instrumentation: The experimental setup was similar to the one previously described.[6, 7, 10] The cell consisted of a Petri dish containing about 15 mL of solution. It was placed over the stage of an inverted microscope (Axiovert 135, Carl Zeiss) under an argon atmosphere. A charge-coupled-device video camera (VCB-3512, Sanyo), connected to a video monitor (VM-2512, Sanyo) was used to ease the follow-up of the experiments. For all measurements, a four-electrode cell was set up and connected to an integrated potentiostat (Autolab, PGStat 30) equipped with a bipotentiostat module. The reference electrode (SCE, Tacussel Radiometer) was placed into the solution through a salt bridge. The counter electrode consisted of a platinum coil about 1 cm^2 in area. The working electrode was a Pt disk electrode 1.4 mm in diameter made by a cross section of a Pt wire (1 mm diameter) sealed into soft glass and polished at an angle of 45°. The probing electrode was a Pt disk microelectrode about 5 μm in diameter. It was obtained by first pulling a glass capillary (GC120-10, Clark Instruments) with a micropuller (PC-10, Narishige). Then a Pt wire of 25 μm diameter (Good Fellow) was etched and sealed into this capillary by a Bunsen burner flame.[7] Finally, the tip of the capillary was polished at an angle of 45° over a diamond whetstone microgrindler (EG-40, Narishige). Electrical contact was performed with a drop of mercury and a nichrome wire.

The working and probing electrodes were positioned by using two three-dimensional micromanipulators (MHW-103, Narishige) so that their active surfaces were parallel one to each other. Measurements with the probe were performed at several positions starting from the center of the working electrode and following a perpendicular axis. The distances between the electrodes could be monitored with an accuracy of ±5 μm. The origin was set experimentally when an electrical contact between the two electrodes was achieved. The constancy of the signal monitored at the probe around the perpendicular axis was experimentally verified near the working electrode surface over a radial distance of about 50 μm. This ensured that no edge effect was accounted for in the measurements reported here. Under such conditions, only planar diffusion occurs, with a progressive interplay of "natural convection" at larger distances.[10]

The working electrode was biased at potentials between the reduction waves of the mediator and the aromatic halide investigated. Measurements were performed when the current at the working electrode reached its steady state limit in the motionless solution. A time delay of 50 s was then fixed before connecting the probing electrode to the bipotentiostat module through a relay. An appropriate potential was applied at the probing electrode for the amperometric detection. For each mediator–aromatic halide couple, two specific potentials were selected to collect each species independently (see experimental illustrations for further details). A sampling time, θ, of 10 ms was chosen to avoid any positive feedback between the two electrodes at short inter-electrode distances[7] and thus to prevent any alteration of the probe response.

Diffusion coefficients: The diffusion coefficients of the mediators and corresponding radical anions were determined by two methods, from the ratio of the steady-state current plateaux determined with a Pt-disk ultramicroelectrode (10 μm radius) and from the square of the Cottrellian amperometric currents monitored at a millimetric Pt disk electrode. For this purpose, authentic solutions of chemically stable radical anions were

0947-6539/01/0713-2938 $ 17.50+.50/0 *Chem. Eur. J.* **2001**, *7*, No. 13

prepared by exhaustive electrolysis of solution of the precursor. We thus measured $D_M = (1.03 \pm 0.05) \times 10^{-5}\,cm^2 s^{-1}$ and $D_{M^-} = (9.7 \pm 0.5) \times 10^{-6}\,cm^2 s^{-1}$ for benzophenone, $D_M = (1.10 \pm 0.05) \times 10^{-5}\,cm^2 s^{-1}$ and $D_{M^-} = (1.03 \pm 0.05) \times 10^{-5}\,cm^2 s^{-1}$ for 1-cyanonaphthalene, $D_M = (9.1 \pm 0.5) \times 10^{-6}\,cm^2 s^{-1}$ and $D_{M^-} = (8.8 \pm 0.5) \times 10^{-6}\,cm^2 s^{-1}$ for 1,3-diphenylisobenzofuran, $D_M = (1.38 \pm 0.05) \times 10^{-5}\,cm^2 s^{-1}$ and $D_{M^-} = (1.27 \pm 0.05) \times 10^{-5}\,cm^2 s^{-1}$ for methyl benzoate, $D_M = (9.4 \pm 0.5) \times 10^{-6}\,cm^2 s^{-1}$, and $D_{M^-} = (9.1 \pm 0.5) \times 10^{-6}\,cm^2 s^{-1}$ for perylene, in which D_M and D_{M^-} refer to the diffusion coefficients of the neutral form of the mediator and of its radical anion, respectively.

It was rather difficult to determine the diffusion coefficient of aromatic halides precisely by direct electron transfer. However, it can be determined at a millimetric Pt disk electrode by redox catalysis with some of the above mediators, whose diffusion coefficients have been previously determined. From the Cottrellian amperometric currents [Eq. (24)] monitored during the catalytic reduction of the aromatic halides, we thus found $D = (1.34 \pm 0.05) \times 10^{-5}\,cm^2 s^{-1}$ for iodobenzene, $D = (9.5 \pm 0.5) \times 10^{-6}\,cm^2 s^{-1}$ for 2-bromonaphthalene, and $D = (1.03 \pm 0.05) \times 10^{-5}\,cm^2 s^{-1}$ for 2-bromopyridine.

Acknowledgements

This work has been supported in part by the CNRS (UMR 8640), the French Ministry of Research and Education (Action Spécifique DGRT N° 97.1502), and by the Ecole Normale Supérieure. O.S. acknowledges the support from the university of Palermo during his stay in Paris. S.S. acknowledges the FWF Austria for a Erwin Schrödinger-Auslandsstipendium (J1840-CHE).

[1] H. Lund, M. A. Michel, J. Simonet, *Acta. Chem. Scand. Ser. B* **1974**, *28*, 901.
[2] C. P. Andrieux, J. M. Savéant in *Investigations of Rates and Mechanisms of Reactions*, C. *Vol. 6*, *4/E*, *Part 2* (Ed.: F. Bernasconi), Wiley, **1986**, p. 305.
[3] H. Lund, K. Daasbjerg, T. Lund, S. Pedersen, *Acc. Chem. Res.* **1995**, *28*, 313.
[4] C. Amatore, F. Bonhomme, J. L. Bruneel, L. Servant, L. Thouin, *J. Electroanal. Chem.* **2000**, *484*, 1.
[5] C. Amatore, F. Bonhomme, J. L. Bruneel, L. Servant, L. Thouin, *Electrochem. Commun.* **2000**, *2*, 235.
[6] C. Amatore, S. Szunerits, L. Thouin, *Electrochem. Commun.* **2000**, *2*, 248.
[7] C. Amatore, S. Szunerits, L. Thouin, J. S. Warkocz, *Electrochem. Commun.* **2000**, *2*, 353.
[8] C. P. Andrieux, C. Blocman, J. M. Dumas-Bouchiat, J. M. Savéant, *J. Am. Chem. Soc.* **1979**, *101*, 3431.
[9] C. P. Andrieux, J. M. Savéant, K. B. Su, *J. Phys. Chem.* **1986**, *90*, 3815.
[10] C. Amatore, S. Szunerits, L. Thouin, J. S. Warkocz, *J. Electroanal. Chem.* **2001**, *500*, 62.
[11] C. P. Andrieux, J. M. Savéant, *J. Am. Chem. Soc.* **1993**, *115*, 8044.

Received: December 27, 2000 [F2964]